Available online at www.sciencedirect.com
ScienceDirect
Journal of Power Sources 180 (2008) 301–308
JOURNAL OF POWER SOURCES
www.elsevier.com/locate/jpowsour

Experimental study on effect of compaction pressure on performance of SOFC anodes

Kongfa Chen [a], Zhe Lü [a,*], Na Ai [a], Xiangjun Chen [b], Xiqiang Huang [a], Wenhui Su [a,c,d]

[a] *Center for Condensed Matter Science and Technology, Harbin Institute of Technology, Harbin 150001, PR China*
[b] *Section for Theoretical Physics, Harbin Institute of Technology, Harbin 150001, PR China*
[c] *Department of Condensed Matter, Jilin University, Changchun 130022, PR China*
[d] *International Center for Material Physics, Academia, Shenyang 110015, PR China*

Received 21 January 2008; accepted 24 January 2008
Available online 12 February 2008

Abstract

NiO/yttria-stabilized zirconia (YSZ) anode substrates were fabricated at two compaction pressures of 200 and 1000 MPa, the particle size distributions of NiO and YSZ were investigated with powders treated under different conditions using a laser scattering technique (Mastersizer 2000, Malvern Instruments) and the effect of compaction pressure on the performance of solid oxide fuel cell (SOFC) anodes was investigated by studying the effect of compaction pressure on compaction density, sintered density, sintering shrinkage behavior, electronic and ionic conductivities. The results of investigation indicated that the SOFC with the anode compacted at a higher pressure exhibited a superior output performance, for example, a single cell with hydrogen as fuel and oxygen as oxidant exhibited excellent maximum power densities of 2.77 and 0.90 W cm^{-2} at 800 and 650 °C, respectively, which suggested the development of an intermediate temperature SOFC through optimization of anode fabrication parameters.

Keywords: Compaction pressure; Anode performance; NiO/YSZ anode; Agglomerate

1. Introduction

Solid oxide fuel cell (SOFC) is one of the most promising electric power conversion systems with high conversion efficiency and low pollution [1]. Numerous studies have been conducted on anode-supported, thin-film electrolyte cells to bring the operation temperature down to an intermediate temperature zone (650–800 °C) in recent years [2–4]. The substantial reduction in the electrolyte thickness causes overall performance of a cell to be dominated by the electrode polarization losses. Compared with a Ni/YSZ (yttria-stabilized zirconia) anode, the electrode polarization from a Sr-doped $LaMnO_3$ (LSM) cathode is quite large [5], which is a primary factor limiting the cell output performance at a reduced temperature.

To date, significant progress has been made in developing high performance LSM-based composite cathodes, such as LSM/YSZ [6], LSM/GDC (gadolinia-doped ceria) [7] and LSM/ScSZ (scandia-stabilized zirconia Co-doped with ceria) [8]. Incorporation of these mixed oxide cathode formulations has done much to reduce the polarization losses with maximum power densities of 2.24 [8] and 2.32 W cm^{-2} [6] at 800 °C. It is predicted that under these circumstances any decrease in the electrode polarization loss will result in a marked enhancement of cell performance. In this sense, the anode polarization cannot therefore be neglected any more.

An anode provides an electrochemical reaction site for the oxidation of fuel and allows the fuel and byproducts to be delivered and removed from the surface site [9]. The performance of an anode is critically dependent on its microstructure [10], which in turn is closely dependent on the starting powder preparation and anode forming processes [9,10].

Uniaxial die compaction is the simplest form of consolidation process extensively used to densify powder materials [11]. NiO/YSZ composite powder is usually compacted in this way to form the small button anode substrates used for laboratory study. As one of the most contributing processing parameters, compaction pressure has its significant effect on the microstructure

* Corresponding author. Tel.: +86 451 86418420; fax: +86 451 86412828.
E-mail addresses: explorer_081@163.com (K. Chen), lvzhe@hit.edu.cn (Z. Lü).

0378-7753/$ – see front matter © 2008 Elsevier B.V. All rights reserved.
doi:10.1016/j.jpowsour.2008.01.072

Table 1
Parameters of powder samples

Denotation	Compaction pressure (MPa)	Grinding time (h)
NiO-r	0	0
NiO-g	0	2
NiO-p1	200	2
NiO-p2	1000	2
YSZ-r	0	0
YSZ-g	0	2
YSZ-p1	200	2
YSZ-p2	1000	2

of anodes. For example, Lee et al. [12] found the microstructure and electrical properties of anodes could be easily manipulated using a compaction pressure ranging from 2 to 7 MPa. Rajaram et al. [13] investigated the influence of compaction pressure on the porosity of an anode. However, to the best of our knowledge, not much work has been done on the effect of compaction pressure on the performance of an anode and even not an anode supported single cell has been fabricated and measured to determine whether such an anode is useful.

Therefore, we compacted NiO/YSZ anode substrates at two different pressures 200 and 1000 MPa, the particle size distributions of NiO and YSZ were investigated with powders treated under different conditions and the effect of compaction pressure on the performance of SOFC anodes was investigated by studying the effect of compaction pressure on compaction density, sintered density, sintering shrinkage behavior, electronic and ionic conductivities. The results of investigation indicated that the SOFC with the anode compacted at a higher pressure exhibited a superior output performance.

2. Experimental

Raw NiO powder was synthesized by the precipitation method [14] and calcined at 1000 °C for 2 h. The raw NiO, commercial YSZ (TZ-8Y, Tosoh Corp.) and wheat starch used as the pore-formers were mixed at a weight ratio of 5:5:2.5, and pestled in a mortar for 2 h to form the green anode powder. The anode powder was then pressed into pellets of 13 mm in diameter and about 0.6 mm in thickness at two uniaxial compaction pressures 200 and 1000 MPa. The compacts were then pre-calcined at 1000 °C for 2 h to attain the anode substrates Anodes-1 and -2. For comparison, the anodes without pore-formers were also compacted at 200 and 1000 MPa to attain anode substrates Anodes-r1 and -r2, respectively.

In order to investigate the evolution of particle size in different treating processes, raw NiO powder and commercial YSZ powder were pressed into pellets at different compaction pressures and then ground in a mortar for 2 h. For comparison, powders, which had been directly ground for 2 h, were also prepared. The particle size distributions of raw powders and treated powders were measured using a laser scattering technique Mastersizer 2000, Malvern Instruments (see Table 1 below for further details of the powders).

The as-prepared anode substrates were cut in the dimensions of 5.0 mm × 5.0 mm × 0.6 mm. The sintering shrinkage behavior of these rectangle anodes was tested using a dilatometer (DIL 402C/3/G, Netzsch) at a constant heating rate of 5 °C min^{-1} from 50 to 1400 °C. The sintering shrinkage behavior of NiO and YSZ cylinders pressed at 200 MPa (6 mm in diameter and 4–5 mm in thickness) was also measured for comparison.

The DC electrical conductivities of the anodes sintered at 1400 °C for 2 h after their reductions were measured in hydrogen by a four-probe method using a sourcemeter (Keithley 2400). Upon the completion of the test, the nickel was removed from the Ni/YSZ anodes by acid leaching to attain the YSZ matrixes. The Ni/YSZ samples were soaked in a HNO_3 solution at about 80 °C for 2 h. After being washed and dried, the DC ionic conductivity of these porous YSZ matrixes was measured by the same four-probe method. The sample measured about 5.5 mm × 3.8 mm × 0.5 mm.

After compaction and sintering at different temperatures, the apparent densities of anodes were determined by weight and dimensions.

The YSZ films were coated onto the anode substrates by the slurry spin coating technique [15]. The bilayers were then co-fired at 1400 °C for 2 h. A $La_{0.7}Sr_{0.3}MnO_3$/$Sm_{0.2}Ce_{0.8}O_{1.9}$ (LSM/SDC) composite cathode was fabricated on the YSZ films by the SDC-impregnation method [16]. The effective cathode area was 0.15 cm^2. The Anodes-1 and -2 based cells were denoted as Cells-1 and -2, respectively. A silver paste (DAD-87, Shanghai Research Institute of Synthetic Resin, China) was employed as both the current collector and the sealing material. After being sealed, the cells were tested using the four-probe method in an electrical furnace. The NiO/YSZ anode was reduced in situ at 800 °C. The anode was fed with hydrogen at 200 ml min^{-1} and the cathode was exposed to an oxygen flow at 100 ml min^{-1}. The *I–V* characteristics and ac impedance spectra of these cells were measured with an electrochemical interface Solartron SI 1287 and an impedance analyzer SI 1260 at a temperature in the range of 650–800 °C.

The microstructures of anodes were characterized using a scanning electron microscope (SEM, S-570, Hitachi). The microstructure of Anode-0 compacted at about 80 MPa was also characterized for comparison.

3. Results and discussion

Particles with fine grains are usually easy to form agglomerates, and they are usually composed of multiple generations of agglomerates [17,18]. The first generation is the cluster of crystallites, namely, domains, and the second generation is the cluster of domains. Successive generations are clusters of former generations at higher scales. In reality, the particle size of agglomerates would be significantly changed by the consolidation forces [17]. So, the particle size distributions of NiO and YSZ powders treated under different conditions were measured, as shown in Fig. 1.

As shown in Fig. 1a, the raw NiO powder (NiO-r) is distributed within a range from about 0.3 μm to 200 μm. After grinding, the particle size distribution range is considerably nar-

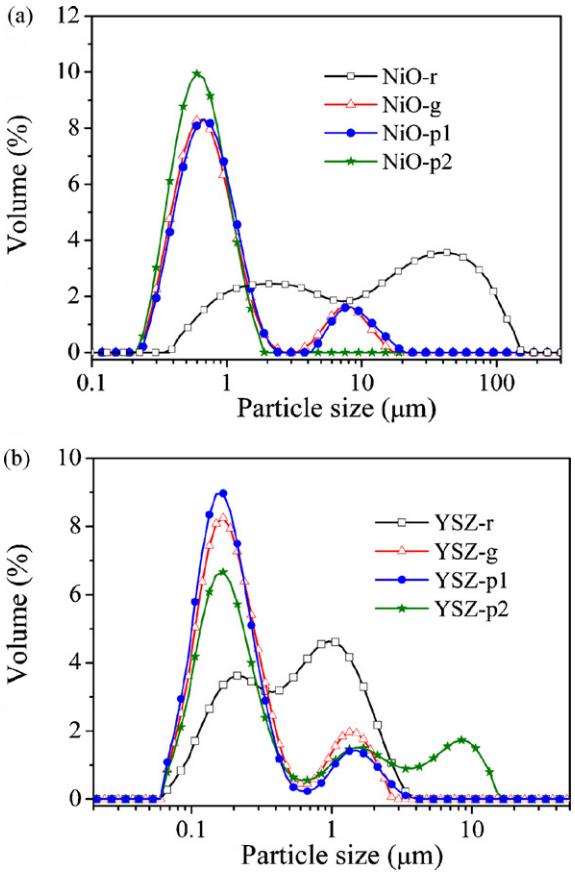

Fig. 1. Particle size distribution of powders in different treating processes: (a) NiO and (b) YSZ.

rowed from about 0.2 to 20 μm (see NiO-g), which means that the bonds between large generations of agglomerates can be easily destroyed by a usual grinding operation. On the other hand, the bimodal distribution of NiO-g at 0.6 and 8 μm indicates that the powder is still composed of several lower generations of agglomerates. The application of 200 MPa has no effect on the powder size distribution (see NiO-p1). Whereas, the large agglomerates at 8 μm disappear when a compaction pressure of 1000 MPa was applied (see NiO-p2), which means that the bonds within the large agglomerates could still be destroyed by the additional high stress, while the bonds within the agglomerates at 0.6 μm are too strong to be destroyed.

As shown in Fig. 1b, the as-received commercial YSZ powder shows a bimodal distribution at 0.2 and 1 μm. Most of the large agglomerates at 1 μm are reduced to 0.2 μm through grinding (see YSZ-g). Compared with YSZ-g, the application of 200 MPa slightly reduces the agglomerates at 1 μm, while the size distribution is slightly widened (see YSZ-p1). Surprisingly, a third peak at 9 μm appears after the application of 1000 MPa (see YSZ-p2). A new higher generation of agglomerates has been formed at a higher pressure, and they could not be destroyed by the following grinding operations. This indicates that the bonds between the YSZ particles have been improved by the higher pressure applied, and the particle size evolution of NiO particles is different from that of YSZ particles.

The green anode powder was prepared by grinding the as-prepared raw NiO powder (NiO-r) and the as-received commercial YSZ (YSZ-r) together. Hence, the particle size distributions of NiO and YSZ powders in the green anode powder are similar to those of NiO-g and YSZ-g. In addition, the particle size distributions of NiO-p1, NiO-p2, YSZ-p1 and YSZ-p2 can be useful as a reference to estimate the changes in particle size during the compaction of anode substrates.

The green anode powder was compacted at 200 and 1000 MPa. It can be seen from Table 2 that the green compaction density increases as the compaction pressure increases. The compaction pressure causes the deformation of soft agglomerates via the rearrangement of primary constituents [17]. Furthermore, the interagglomerate pores are also filled through the sliding and rearrangement of lower generations of agglomerates. These processes help the compaction of loose powder. Apparently, a denser compact can be produced using a higher compaction pressure. After being pre-calcined at 1000 °C, the organic pore-formers have been burned out, and the compact density also increases as the compaction pressure increases. After being sintered at 1400 °C, the anode is much denser than that after being pre-calcined at 1000 °C. However, to our great surprise, the density of Anode-1 is then higher than that of Anode-2 after being sintered at 1400 °C. This unusual result is different from the results obtained by other authors [17–19]. The possible explanation for this is that different sintering and densification processes might occur between 1000 and 1400 °C. So, we measure the sintering shrinkage behaviors of anodes to further explore the cause at the root.

Fig. 2a shows the sintering shrinkage curves of anodes, which have been already pre-calcined at 1000 °C before measurements. Fig. 2b shows the sintering shrinkage rate curves of anodes, which are the derivatives of sintering shrinkage curves. Since the heating rate is constant, temperature instead of time can be *x*-axis variable. As shown in Fig. 2a, the linear shrinkage of Anode-1 is about 7.0% larger than that of Anode-2 between 1000 and 1400 °C. A larger sintering shrinkage is prone to resulting in a higher sintered density. As shown in Fig. 2b, significant shrinkage rates appear at three different temperatures of 1180, 1275 and 1350 °C for Anode-1. The absolute values of shrinkage rate in Anode-1 are generally higher than those of Anode-2. Moreover, compared to the peaks of Anode-1, the first peak of Anode-2 appears later and both the second and third peaks of Anode-2 appear earlier.

Table 2
Apparent density of anodes sintered at different temperatures

Sample	Compaction density (g/cm^3)	Relative density, calcined at 1000 °C (%)	Relative density, sintered at 1400 °C (%)
Anode-1	2.52	34.0	67.6
Anode-2	2.81	37.8	62.7

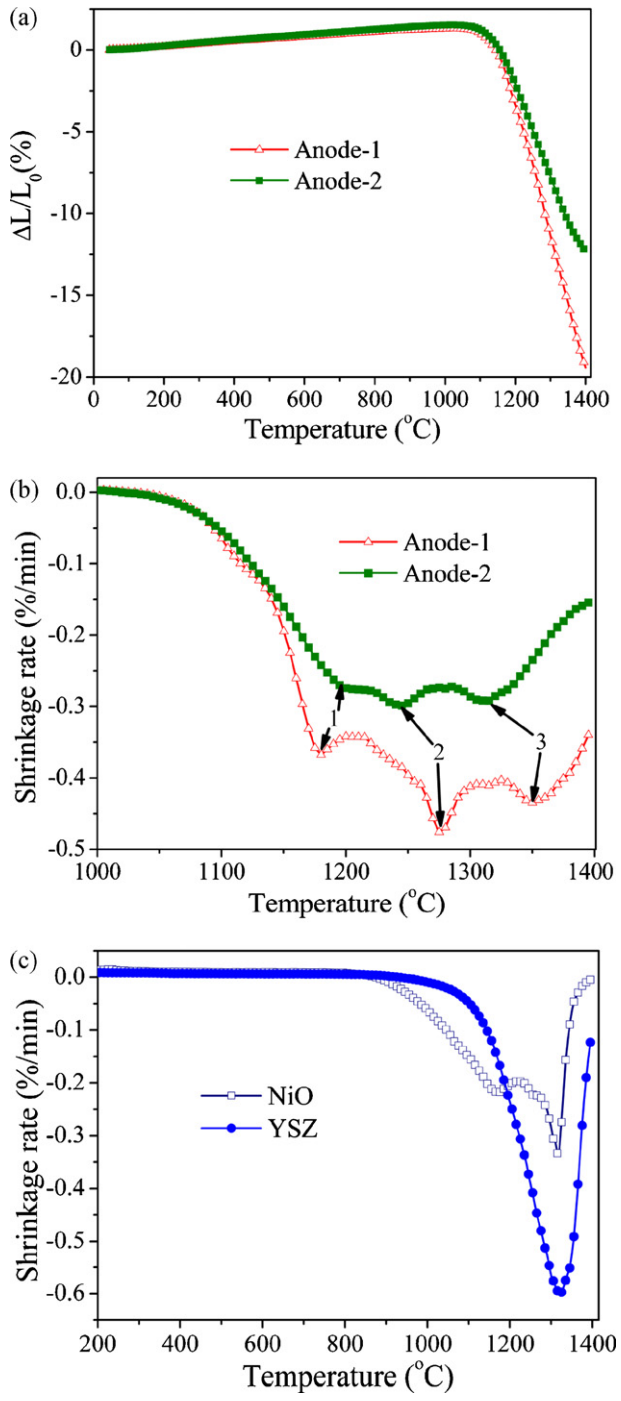

Fig. 2. (a) Sintering shrinkage of anodes, (b) sintering shrinkage rate of anodes, and (c) sintering shrinkage rate of NiO and YSZ samples.

For single phase solid systems, sintering and densification are the process of pore elimination and particle rearrangements, which are usually divided into three stages: the first stage is the sintering within the hard agglomerates, the second one is surface and grain boundary diffusions within the soft agglomerates, and the last one is mass diffusion [20]. Often, the first sintering stage occurs at a temperature below 1000 °C, since the packing density of hard agglomerates is sufficient that sintering will readily occur at a lower temperature. Consequently, the peak of the shrinkage rate curves associated with the first sintering stage could not be observed in the anodes pre-calcined at 1000 °C, and only the last two peaks could be observed.

Fig. 2c shows the sintering shrinkage rate curves of NiO with the as-prepared raw powder as the precursor and YSZ with the as-received commercial powder as the precursor. The cylinder samples were pressed at 200 MPa, followed by sintering shrinkage measurement. The NiO cylinder exhibits two peaks at 1172 and 1315 °C. The YSZ cylinder shows an asymmetric single peak at 1323 °C. No significant shrinkage rate can be observed in either of the two samples at a temperature below 1000 °C, since the sintering within the hard agglomerates has already occurred at a high powder pre-heating temperature, for example, 1000 °C for pre-heating of raw NiO powder. As indicated in our recent work [21], the peak of NiO at 1172 °C corresponds to the sintering within the highest generation of agglomerates and the peak of NiO at 1315 °C corresponds to the final densification process. As for YSZ, the single peak at 1323 °C possibly correlates with the final densification process, since the ceramic made of Tosoh 8YSZ powder can be well densified at a temperature above 1300 °C [22]. In fact, after the sintering shrinkage measurements, the apparent density of YSZ cylinder, which was heated to 1400 °C without holding, is about 93%.

With respect to the shrinkage rate curves of NiO and YSZ, both Peak-1 and Peak-2 in Fig. 2b are likely to be generated by the sintering and densification of NiO, and Peak-3 in Fig. 2b is possibly caused by the sintering and densification of YSZ. As shown in Fig. 1a, the soft agglomerates in NiO-p1 could be destroyed at a pressure of 1000 MPa. This makes the sintering within the soft agglomerates more difficult to occur, and therefore delays the appearance of Peak-1 in Anode-2. On the other hand, the fragmentation of soft agglomerates improves the uniformity of particle distribution in the compact, and facilitates the densification process [18], which leads to the earlier appearance of Peak-2 in Anode-2. It can be seen from Fig. 1b that some large YSZ particles would be formed in Anode-2 because the pores between the hard agglomerates of YSZ particles are eliminated. Furthermore, more interagglomerate pores in the ceramic body have been eliminated at a higher pressure during compaction. This is also a contributing factor in facilitating the mass transfer, leading to the earlier appearance of Peak-3 in Anode-2.

It can be seen from the discussion concerning the sintering shrinkage behaviors that the densification process benefits from the higher compaction pressure. However, the data presented in Table 2 indicates that Anode-2 is actually less dense than Anode-1 when fully consolidated at 1400 °C. This problem could be gradually solved using the anodes without pore-formers and/or pore-formers.

After being pre-calcined at 1000 °C, the density of anodes without pore-formers increases as the compaction pressure increases, e.g., the density of Anode-r2 is 12.2% higher than that of Anode-r1. After being sintered at 1400 °C without holding, the density of anodes also increases as the compaction pressure increases, e.g., the density of Anode-r2 is 4.3% higher than that of Anode-r1, which coincides with the findings reported in the literature [17–19].

As shown in Fig. 3a, there are small and large pores in the anodes with pore-formers. In general, larger pores and more

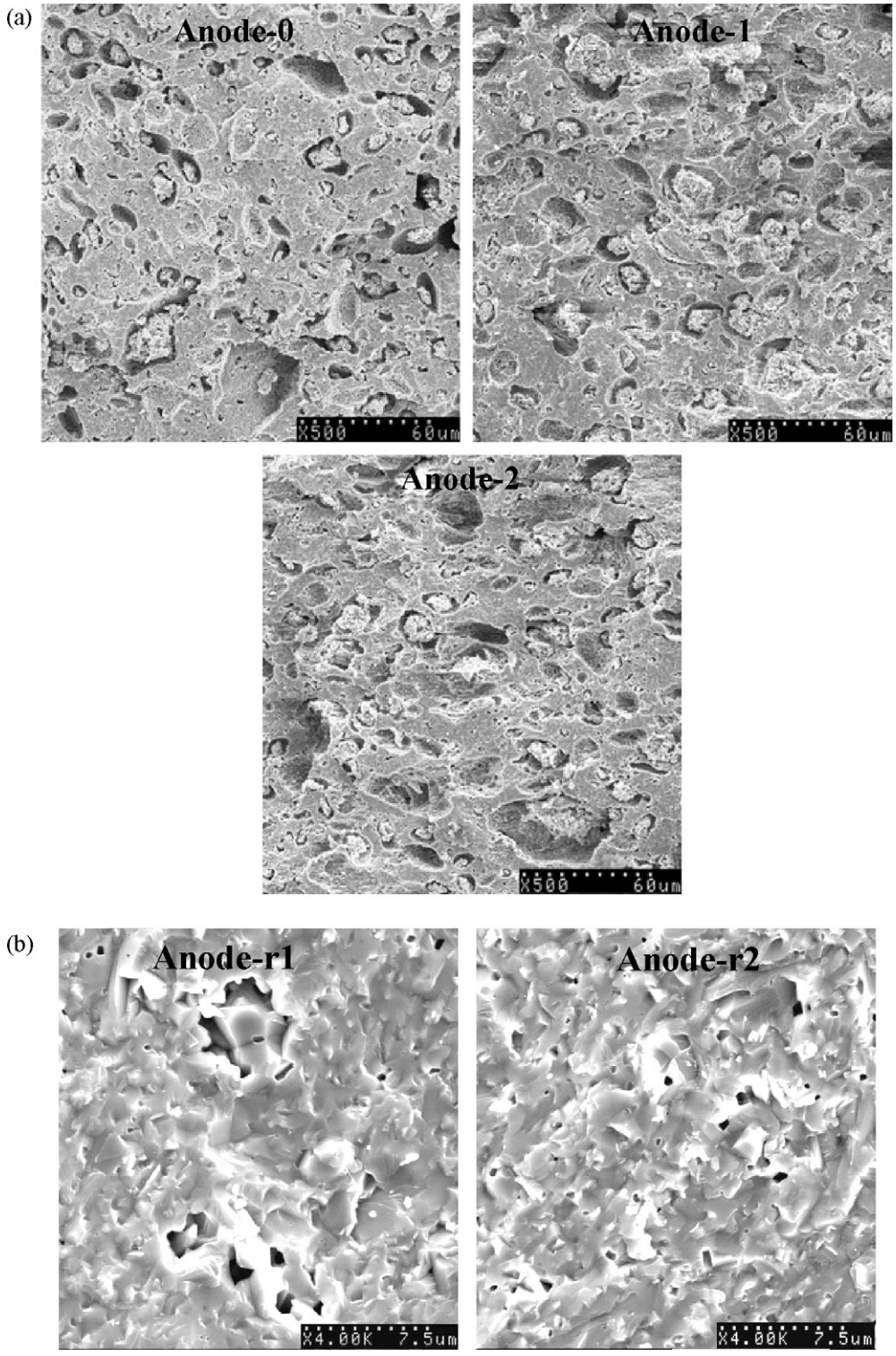

Fig. 3. Fractured images of (a) Anode-0, Anode-1 and Anode-2 with pore-formers and (b) Anode-r1 and Anode-r2 without pore-formers. The anodes were sintered at 1400 °C.

pores are produced at a higher compaction pressure. Smaller pores are produced by incomplete densification, while larger pores are produced in the anode during the burnout of pore-formers. It can be seen from Fig. 3b that there are some cracks and pores in Anode-r1, and the microstructure of Anode-r2 is more homogeneous. The development of cracks and formation of pores in Anode-r1 is mainly caused by the higher generations of agglomerates in NiO, which have been destroyed in Anode-r2 by a higher compaction pressure. This results in the sintered density of Anode-r2 higher than that of Anode-r1. The dense solid part of the anode with pore-formers should be similar to that of the anode without pore-formers. So, the dense solid part

of Anode-2 should be denser than that of Anode-1. In this sense, a higher compaction pressure facilitates the sintering and densification in the solid part of an anode, and a higher volume ratio of larger pores causes the additional porosity of Anode-2.

The pore-formers in anodes should be smaller in volume when a higher compaction pressure is used, and most of the pores in Anode-2 are smaller in size than those in Anode-1 at 1000 °C. It is generally accepted that mass diffusion is a process of pore elimination. The coordination number (R) of a pore determines whether the pore can eventually disappear through mass diffusion [17]. Only the pores with R blow R_c, critical coordination number, can disappear in the sintering and densification process. Compared with Anode-1, the pores in Anode-2 have a higher coordination number, because there are more particles packed in a given space at a higher pressure. So, the grow rate of pores in Anode-2 should be higher than that of the particles in Anode-2, and causes the generation of more thermodynamically stable pores in Anode-2 which could not be eliminated at a higher sintering temperature. After being sintered at 1400 °C, the pores in Anode-2 are larger in size by average and there are more pores in Anode-2 as well, which causes a higher porosity in Anode-2 than Anode-1. This explains the abnormality in the relative densities of Anodes-1 and -2 as a function of sintering temperature.

It can be seen from Fig. 4a that the electrical conductivity of anodes after reduction decreases with temperature, because a continuous Ni metal conducting path has been formed. The conductivity of Anode-2 is slightly higher than that of Anode-1. Upon completion of the conductivity experiments, acid leaching was used to remove the nickel from the Ni/YSZ anode before the ionic conductivity of YSZ matrixes was conducted. As shown in Fig. 4b, the conductivity of YSZ matrixes increases as the temperature increases, as the result of the formation of a continuous ionic conduction path in the anodes. The two anodes exhibit similar ionic conductivities. From these data it is evident that higher compaction pressures are associated with an increase in the electronic conductivity but appear to have no impact on the ionic conductivity in the cermet compacts.

The existence of pores would result in either diminished ionic or electrical conductivities, since they have occupied the place where there otherwise would have nickel or YSZ particles to provide electrical connection [23]. In this sense, the greater porosity in Anode-2 would result in both lower electronic and ionic conductivities. On the other hand, the larger YSZ particles in Anode-2 formed during compaction help the connection of NiO particles [24], and improve the particle-to-particle connection of YSZ particles. It can be seen from the conductivity results that the disadvantages of increased porosity has been inhibited by the advantages of larger YSZ particles in Anode-2. In addition, the denser solid part in Anode-2 is also a contributing factor in promoting the electrical conductivity. As is readily observed, it is desirable to maximize porosity and pore size assuming that other pertinent factors are unaffected (e.g., conductivity, integrity, strength, etc.).

As shown in Fig. 5, the dense YSZ film is about 8 μm thick, and it coheres well to the anode substrate, and the cathode adheres to the YSZ intimately. Some of the large pores in the anode are close to the YSZ film. These pores would diminish

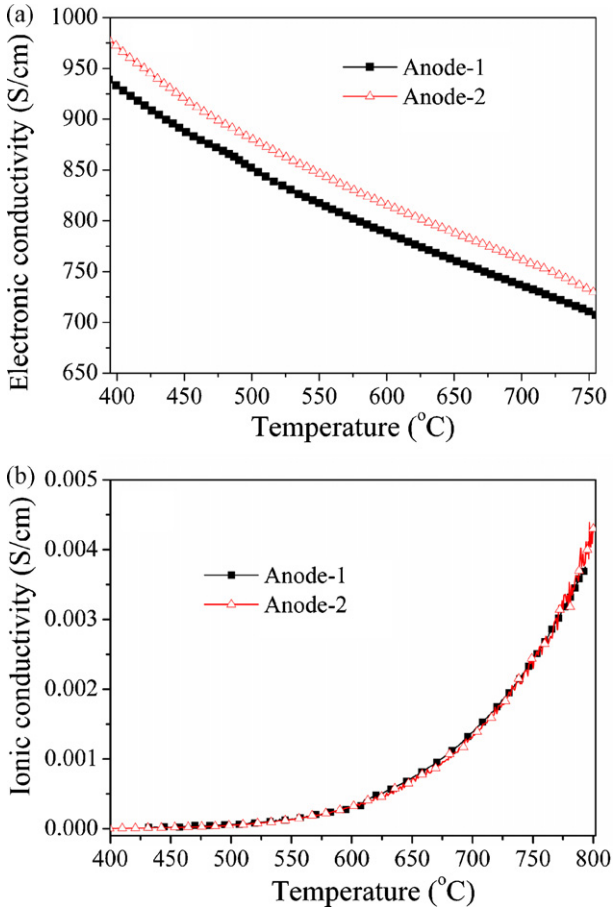

Fig. 4. (a) Electronic conductivities and (b) ionic conductivities of two anodes.

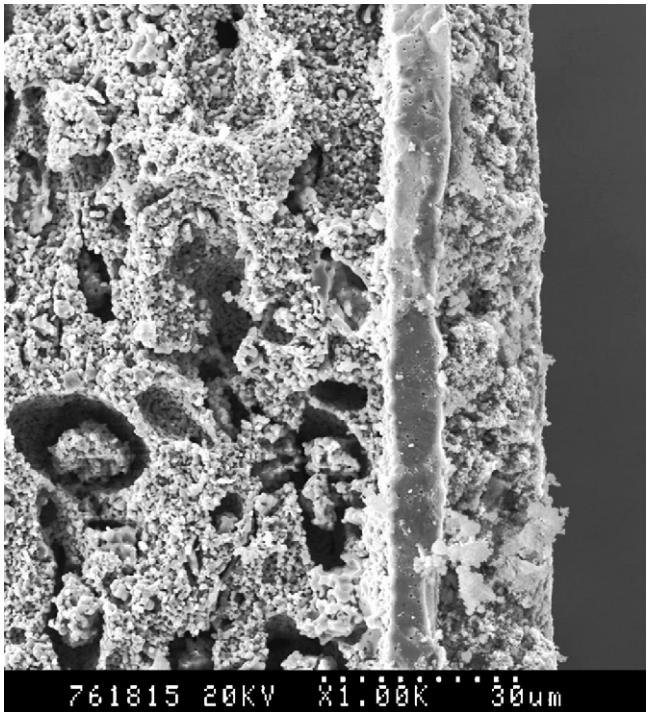

Fig. 5. A typical fractured image of Cell-1 after electrochemical testing.

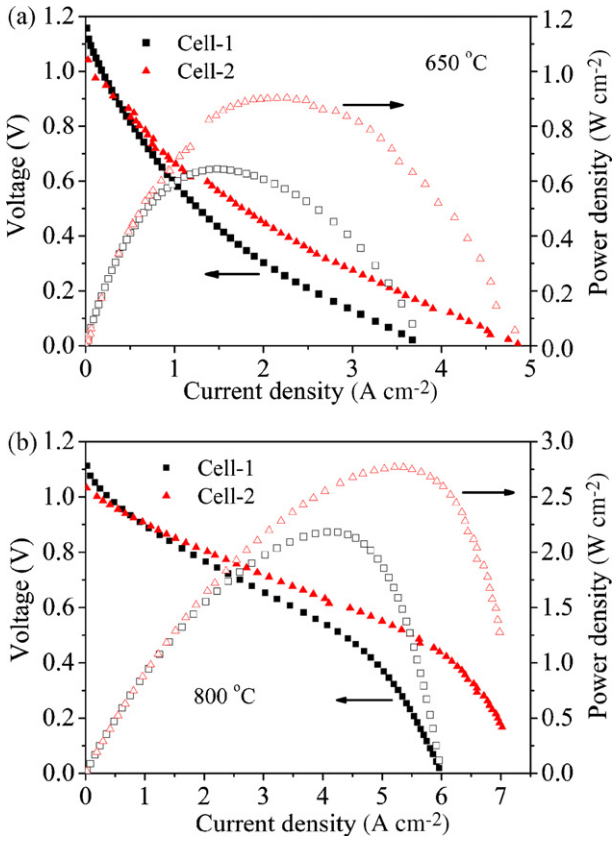

Fig. 6. Electrochemical characteristics of the two cells based on the anodes compacted at different pressures.

the overall three-phase boundary (TPB) sites in the very effective thickness of the reaction area adjacent to the YSZ film and reduce the area available for chemical reaction [23]. This is detrimental to the enhancement of anode performance. In the case of Anode-2, the additional large pores in the anode/YSZ interface would result in additional loss of TPBs. We have planned to fabricate a fine anode functional layer (AFL) to reduce the number of pores in the interface [25].

Fig. 6 shows both cells yield desirable output performances at 800 °C, and Cell-2 exhibits much better output performance than that of Cell-1. The maximum power densities of cells at different temperatures are tabulated in Table 3. The higher performance of Cell-2 indicates that the performance of a reduced temperature SOFC with YSZ electrolyte can be improved by optimizing the anode fabrication parameters.

The YSZ films and the LSM/SDC composite cathodes were fabricated using the same processes. In addition, at least two cells with the same fabrication processes were tested to warrant the good reproducibility. Hence, the difference in cell performance and overall electrode polarization losses can be attributed to the difference in anodes.

Table 3
Maximum power densities of Cell-1 and Cell-2 at different temperatures

Temperature (°C)	MPD of Cell-1, P_1 (W/cm^2)	MPD of Cell-2, P_2 (W/cm^2)	$(P_2 - P_1)/P_1$ (%)
800	2.19	2.77	26.5
750	1.75	2.29	30.9
700	1.14	1.61	41.2
650	0.64	0.90	40.6

The limitation on the performance of an anode is based on both activation and concentration polarizations. Activation polarization is related to the charge transfer process and depends on the amount of TPB, and concentration polarization is related to the mass transfer process and mainly depends on the anode porosity [9]. The output performance is low at a low temperature, e.g., 650 °C, and so, low anode porosity is sufficient for rapid transport of fuel gas and byproducts. This suggests that the mass transfer process is not the rate-determining step (rds) dominating the output performance of a cell at a high current density, and the charge transfer process is predominant at this time. The high performance of Cell-2 indicates the lengthened TPB of Anode-2 is associated with the evolution of particle size with the different compaction pressures. It can be seen from Fig. 1a that fine NiO particle (0.6 μm) are generated through the fragmentation of large agglomerates (8 μm) at a higher pressure. The sliding and rearrangement of fine NiO particles created more contacts between YSZ and NiO particles. It can also be seen from Fig. 1b that fine YSZ particles (0.2 μm) form stable coarse YSZ particles (9 μm) at a higher pressure. The combination of fine and coarse YSZ particles facilitates the formation of a more stable YSZ frame and Ni network [24], which results in substantially improved stability and performance of Ni/YSZ anode [10]. Greater porosity increases the hydrogen concentration in Anode-2, providing more hydrogen molecules to contact Ni particles, and it also accelerates the gas exchange within the anode and causes the trapped vapor to diffuse more rapidly from the effective anode layer. These factors promote the performance of Anode-2, thereby promoting the performance of Cell-2 at 650 °C.

The temperature-dependent electrode polarization loss and ohmic loss is much lower at an elevated temperature, e.g., 800 °C. Consequently, the potential performance of a cell is much higher. The anode concentration polarization would occur at a critical current density (i_c) for a given anodic porosity. In this case, vapor is abundant but fuel is insufficient in an anode, which leads to the rapid drop of cell voltage. Under this condition, the mass transfer process becomes the rds. The greater porosity of Anode-2 reduces the anode concentration polarization and boosts the performance of a cell at a high current density. On the other hand, it was found that the shortage of TPB to support the rapid chemical reaction at a high current density is also responsible for the concentration polarization-like phenomenon, even though the fuel gas is sufficient. This determination is based on another publication not yet available for reference. So the advantages of Anode-2, such as fast electrochemical reaction and sufficient porosity, result in the superior performance of Cell-2 at 800 °C.

The curves shown in Fig. 7 contains both anode and cathode polarizations. The cathode polarization losses in two cells are identical to each other since the cathodes were fabricated with the same process. Hence, the difference in the two curves shown in Fig. 7a is due to the difference in the performance of anodes. Obviously, Anode-2 has much lower anode polarization than

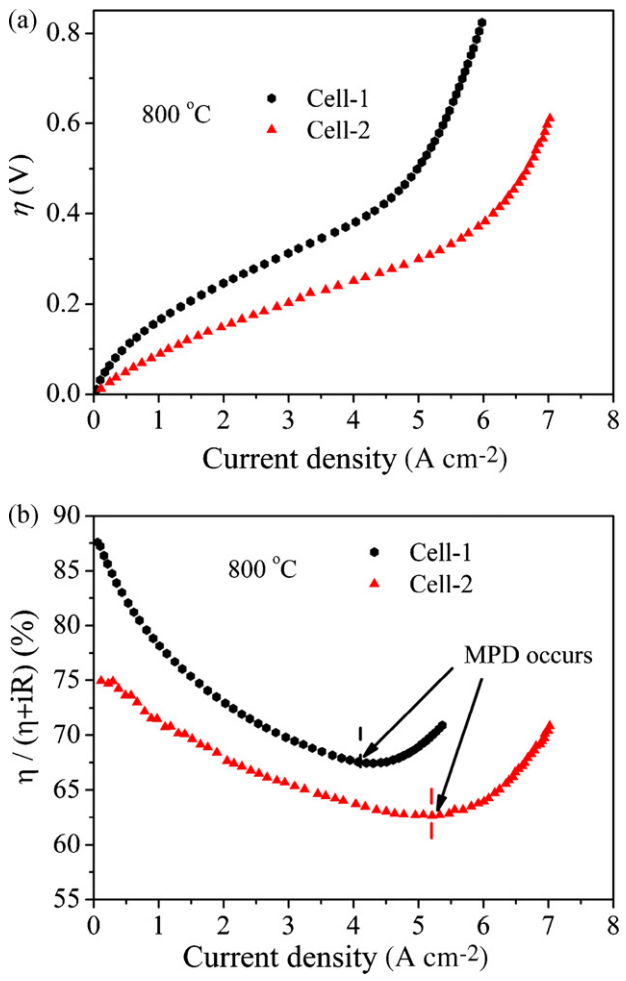

Fig. 7. (a) Electrode polarization loss and (b) ratio of the electrode polarization loss in total cell polarization loss as a function of current density at 800 °C.

that of Anode-1. As shown in Fig. 7b, there is a peak in the curve, which suggests the shift of rds from the charge transfer process to the mass transfer process. The η% values of Cell-2 are lower than those of Cell-1. It can be seen from Fig. 7b that the η% values at MPD, are 68 and 62% for Cell-1 and Cell-2, respectively. As a summary, the electrode polarization loss can be reduced at a higher compaction pressure, which leads to the improvement of anode performance.

4. Conclusions

It can be seen from the results and discussion above that:

1. Although the particle size distribution in the agglomerates of ground NiO and YSZ powders remained at a lower compaction pressure, the large generation of agglomerates in NiO powder was destroyed at a higher compaction pressure while a large generation of agglomerates in YSZ powder was formed at a higher compaction pressure;
2. the packing density, sintered density and sintering shrinkage of anodes could be manipulated by changing the compaction pressure;
3. a higher compaction pressure is associated with an increase in the electronic conductivity but it has no impact on the ionic conductivity in the cermet compacts; and
4. the single cell with an anode compacted at a higher compaction pressure exhibited a superior cell performance.

Acknowledgements

The authors thank the Ministry of Science and Technology of China (contract no. 2007AA05Z139) for its financial support, Zhengqian Luo, Department of Communication Engineering, Xiamen University, China and Dan Bing, Division of Physics & Applied Physics, Nanyang Technological University, Singapore for their assistances.

References

[1] S. Suda, M. Itagaki, E. Node, S. Takahashi, M. Kawano, H. Yoshida, T. Inagaki, J. Eur. Ceram. Soc. 26 (2006) 593–597.
[2] J. Will, A. Mitterdorfer, C. Kleinlogel, D. Perednis, L.J. Gauckler, Solid State Ionics 131 (2000) 79–96.
[3] R.Q. Yan, D. Ding, B. Lin, M.F. Liu, G.Y. Meng, X.Q. Liu, J. Power Sources 164 (2007) 567–571.
[4] N. Ai, Z. Lü, K.F. Chen, X.Q. Huang, Y.W. Liu, R.F. Wang, W.H. Su, J. Membr. Sci. 286 (2006) 255–259.
[5] S. de Souza, S.J. Visco, L.C. De Jonghe, Solid State Ionics 98 (1997) 57–61.
[6] K.F. Chen, Z. Lü, X.J. Chen, N. Ai, X.Q. Huang, X.B. Du, W.H. Su, J. Power Sources 172 (2007) 742–748.
[7] S.P. Jiang, W. Wang, Solid State Ionics 176 (2005) 1351–1357.
[8] Z.W. Wang, M.J. Cheng, Y.L. Dong, M. Zhang, H.M. Zhang, Solid State Ionics 176 (2005) 2555–2561.
[9] W.Z. Zhu, S.C. Deevi, Mater. Sci. Eng. A 362 (2003) 228–239.
[10] S.P. Jiang, S.H. Chan, J. Mater. Sci. 39 (2004) 4405–4439.
[11] P. Chen, G.Y. Kim, J. Ni, J. Mater. Process. Technol. 190 (2007) 243–250.
[12] D.S. Lee, J.H. Lee, J. Kim, H.W. Lee, H.S. Song, Solid State Ionics 166 (2004) 13–17.
[13] G. Rajaram, Z. Xu, X. Jiang, D.M. Pai, J. Filatovs, J. Sankar, Ceram. Eng. Sci. Proc. 26 (4) (2005) 177–183.
[14] K. Chen, et al., J. Alloys Compd. 454 (2008) 447–453.
[15] K.F. Chen, Z. Lü, N. Ai, X.Q. Huang, Y.H. Zhang, X.D. Ge, X.S. Xin, X.J. Chen, W.H. Su, Solid State Ionics 177 (2007) 3455–3460.
[16] K.F. Chen, Z. Lü, N. Ai, X.J. Chen, J.Y. Hu, X.Q. Huang, W.H. Su, J. Power Sources 167 (2007) 84–89.
[17] F.F. Lange, J. Am. Ceram. Soc. 67 (1984) 83–89.
[18] B.C. Kim, J.H. Lee, J.J. Kim, J. Eur. Ceram. Soc. 27 (2007) 807–812.
[19] L. Gao, W. Li, H.Z. Wang, J.X. Zhou, Z.J. Chao, Q.Z. Zai, J. Eur. Ceram. Soc. 21 (2001) 135–138.
[20] R.Q. Yan, F.F. Chu, Q.L. Ma, X.Q. Liu, G.Y. Meng, Mater. Lett. 60 (2006) 3605–3609.
[21] K.F. Chen, X.J. Chen, Z. Lü, N. Ai, X.Q. Huang, W.H. Su, Effect of preheating temperature on characteristics of NiO powder and its compact, Int. J. Appl. Ceram. Technol. (submitted for publication).
[22] Y.H. Zhang, X.Q. Huang, Z. Lu, Z.G. Liu, X.D. Ge, J.H. Xu, X.S. Xin, X.Q. Sha, W.H. Su, J. Power Sources 160 (2006) 1065–1073.
[23] J.J. Haslam, A.Q. Pham, B.W. Chung, J.F. Dicarlo, R.S. Glass, J. Am. Ceram. Soc. 88 (2005) 513–518.
[24] H. Itoh, T. Yamamoto, M. Mori, T. Horita, N. Sakai, H. Yokokawa, M. Dokiya, J. Electrochem. Soc. 144 (1997) 641–646.
[25] N. Ai, Z. Lü, K.F. Chen, X.Q. Huang, X.B. Du, W.H. Su, J. Power Sources 171 (2007) 489–494.